Directional sensing in eukaryotic chemotaxis: A balanced inactivation model

Herbert Levine, David A. Kessler, and Wouter-Jan Rappel

This information is current as of May 2007.

Online Information & Services	High-resolution figures, a citation map, links to PubMed and Google Scholar, etc., can be found at: www.pnas.org/cgi/content/full/103/26/9761
Supplementary Material	Supplementary material can be found at: www.pnas.org/cgi/content/full/0601302103/DC1
References	This article cites 39 articles, 16 of which you can access for free at: www.pnas.org/cgi/content/full/103/26/9761#BIBL
	This article has been cited by other articles: www.pnas.org/cgi/content/full/103/26/9761#otherarticles
E-mail Alerts	Receive free email alerts when new articles cite this article - sign up in the box at the top right corner of the article or click here.
Rights & Permissions	To reproduce this article in part (figures, tables) or in entirety, see: www.pnas.org/misc/rightperm.shtml
Reprints	To order reprints, see: www.pnas.org/misc/reprints.shtml

Notes:

Directional sensing in eukaryotic chemotaxis: A balanced inactivation model

Herbert Levine*, David A. Kessler†, and Wouter-Jan Rappel*‡

*Center for Theoretical Biological Physics, University of California at San Diego, 9500 Gilman Drive, La Jolla, CA 92093; and †Department of Physics, Bar-Ilan University, Ramat-Gan 52900, Israel

Many eukaryotic cells, including *Dictyostelium discoideum* amoebae, fibroblasts, and neutrophils, are able to respond to chemoattractant gradients with high sensitivity. Recent studies have demonstrated that, after the introduction of a chemoattractant gradient, several chemotaxis pathway components exhibit a subcellular reorganization that cannot be described as a simple amplification of the external gradient. Instead, this reorganization has the characteristics of a switch, leading to a well defined front and back. Here, we propose a directional sensing mechanism in which two second messengers are produced at equal rates. The diffusion of one of them, coupled with an inactivation scheme, ensures a switch-like response to external gradients for a large range of gradient steepness and average concentration. Furthermore, our model is able to reverse the subcellular organization rapidly, and its response to multiple simultaneous chemoattractant sources is in good agreement with recent experimental results. Finally, we propose that the dynamics of a heterotrimeric G protein might allow for a specific biochemical realization of our model.

dynamics | modeling

Chemotaxis is characterized by the directed movement of cells up a chemical gradient and is a key component of a multitude of biological processes, including neuronal patterning, wound healing, embryogenesis, and cancer metastasis (1–3). The sensitivity of eukaryotic cells to gradients can be extremely high: Both neutrophils and the social amoeba *Dictyostelium discoideum* can detect a 1% difference in concentration of the chemoattractant between the front and the back of the cell (4, 5), and recent experiments with growth cones have claimed to exhibit axonal guidance in concentration differences as little as 0.1% (6). Naturally, the question of how internal pathways lead to such a high degree of sensitivity has attracted considerable attention.

Recent research, particularly in *Dictyostelium*, has identified a large number of key components in these pathways, and it has now become possible to draw flow diagrams that link the chemoattractant receptor to the downstream cell behavior, including pseudopod formation and movement (7–10). Even as more and more components of the chemotactic pathways have been discovered, however, it has become clear that the identification of these components is not sufficient to reach a complete understanding of eukaryotic chemotaxis. Underlying this difficulty is the fact that spatial effects within the cells turn out to play a crucial role, leading to mechanisms that are difficult to understand with simple flow diagrams. These spatial effects manifest themselves immediately after a chemoattractant signal. During this initial stage of chemotaxis, commonly referred to as the directional sensing stage (11), subcellular reorganization has been demonstrated in experiments where one or more pathway components are labeled with a fluorescent marker. The time scales associated with this subcellular organization have been measured quantitatively in *Dictyostelium*. A number of the key components, including pleckstrin homology (PH) domain proteins and Ras, localize rapidly (<3 s) and uniformly to the membrane after a gradient stimulation (12–15). This localization

is followed by a nearly total loss of localization at the back of the cell, whereas these components remain localized at the front of the cell (14, 15). It is generally believed that modification of membrane-bound phosphoinositides is responsible for this localization. Indeed, phosphatidylinositol 3-kinase (PI3K) localizes at the front, whereas the phosphoinositide 3 lipid phosphatase PTEN localizes at the opposite side (16–18). Other components that have an asymmetric subcellular pattern include the small GTPase Ras and the p21-activated kinase a (PAKa) (15, 19).

The rapid localization to the membrane, followed by a nearly complete disassociation at the back, suggests that the directional sensing pathway does not merely amplify the external cAMP gradient. Instead, this pathway induces a switch-like behavior, leading to a clearly defined front and back, and does so for a wide range of chemoattractant gradients. This switch-like nature is also evident from recent experiments that carefully measured the fluorescence levels of GFP-tagged PH domain proteins and found that this level approaches zero at the back of the cell (14).

A number of groups, including ours, have performed mathematical modeling studies of chemotaxis in *Dictyostelium* (20–24). The current models, however, do not yet offer a full explanation of the experimental data. For example, the local excitation/global-inhibition model amplifies the external gradient (9, 23, 25) but is unable to address the switch-like behavior discussed above. Our own previous modeling attempt, the "first-hit model," is unable to properly adapt: An internally established gradient is difficult to reverse, and, in addition, the system does not respond properly to sequentially established multiple stimuli (24). Finally, a class of models that exhibit spontaneous symmetry breaking, based on the familiar Turing-pattern paradigm (26), is unable to explain the response of a cell in a small gradient with a high background cAMP level (20, 21, 27). For this type of stimulation, the concentration of cAMP is high all around the cell, modulated by a small perturbation. Turing-type models will exhibit symmetry breaking at the cellular scale with multiple excited regions, and, hence, the activation will not be restricted to the front.

In this article, we present a model for the directional sensing step of eukaryotic chemotaxis. The model takes as input the external cAMP concentration and has as an output an activator field that varies along the membrane and represents a nonlinearly processed counterpart of the external field. We will interpret our results by assuming that this field is directly correlated with the asymmetry visible along the membrane. Our model attempts to incorporate the following experimental findings: (*i*) An external gradient leads to a response of the entire membrane on a time scale of seconds, followed by a loss of localization at the back of the cells within ≈5–10 s; (*ii*) cells are able to reverse

PHYSICS

their internal asymmetry upon reversal of the external chemoattractant gradient direction; and (iii) the cells are able to establish an internal direction over a large range of gradient strengths and background concentration levels.

Our model can be presented and discussed in terms of abstract components, a membrane-bound activator and a diffusing inhibitor. We will, however, also address possible biochemical candidates and, in particular, suggest that a heterotrimeric G protein downstream from the receptor plays a key role in our model. Specifically, we consider the possibility that the two complexes arising from the disassociation of this G protein correspond to the inhibitory and the activatory component of the model. An appeal of our tentative identification of a G protein as the key component in the model is that it solves the "inhibitory puzzle." All models proposed to date rely on the existence of one or more inhibitors that can terminate the response at the back of the cell. However, despite intense research during the past decade, the biochemical identification of the inhibitor(s) is still lacking. A G protein playing the role of both activator and inhibitor eliminates the need for finding a new signal-transduction component.

Results

Response to a Uniform Signal. Let us first look at the steady-state solution resulting from a uniform stimulus S_0. In this case, the concentration of the inhibitor B becomes uniform and is given by

$$B_0 = \frac{k_a S_0}{k_b}. \qquad [1]$$

Then, solving the remaining two equations, we find

$$B_{m,0} = k_b B_0 / (k_i A_0 + k_{-b}),$$

where the concentration of the activator A_0 is given by

$$A_0 = \frac{-k_{-a}k_{-b} + \sqrt{(k_{-a}k_{-b})^2 + 4k_a k_i k_{-a}k_{-b} S_0}}{2k_i k_{-a}}. \qquad [2]$$

We shall see in the following that our mechanism depends on the dimensionless parameter $K \equiv (k_a k_i \bar{S})/(k_{-a}k_{-b})$ being large, with $\bar{S}$ as the average value of S along the cell wall, here being S_0. This condition assures that the overall "balance" between production of activators and inhibitors is only weakly broken by the decay processes; we will assume this throughout. Another way of looking at this is that our mechanism depends on the inhibitor making its way across the cell to modulate the response at the low S end of the cell. If it is ineffective, i.e., if $k_i AB$ is not large enough, because of too slow a production of A and B, too rapid a decay of A or B, or k_i itself being too small, our mechanism will not work. If K is large, Eq. **2** simplifies to

$$A_0 \approx \sqrt{\frac{k_a k_{-\bar{b}}}{k_i k_{-a}}} \sqrt{S_0} = \frac{k_{-b}}{k_i} \sqrt{K}. \qquad [3]$$

Note that, because $A_0 \approx \sqrt{S_0}$, the signal response A is not perfectly adapting. However, the transient response can be much larger than the eventual steady-state level, as can be seen in Fig. 1, where we have plotted the response to a 10-fold increase in S at $t = 0$ s and again at $t = 50$ s.

Response to a Gradient Stimulus. Let us start by considering a simplified one-dimensional geometry; as we will see, all of the main features of our model are also present in this case. We suppose that S is not uniform but is different at the front, S_f, and at the back, S_b, because of an external gradient in the cAMP concentration. Specifically, let us take $S_f = \bar{S}(1 + p)$ and $S_b = \bar{S}(1 - p)$, where p is a dimensionless parameter that characterizes
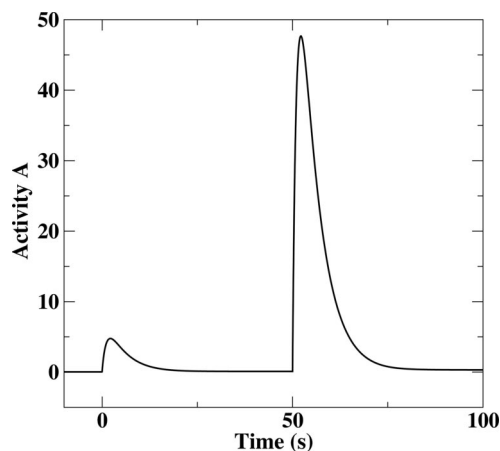

Fig. 1. The response of our model to step-wise changes in uniform concentration of activated receptors. The initial concentration of activated receptors is $S = 1$ molecule per micrometer and is changed 10-fold at $t = 0$ s and another 10-fold at $t = 50$ s. The parameters used are $k_a = 1$ s^{-1}, $k_i = 1,000$ μm (s molecule)$^{-1}$, $k_b = 3$ μm·s^{-1}, $k_{-a} = 0.2$ s^{-1}, $k_{-b} = 0.2$ s^{-1}, and $D = 10$ μm^2·s^{-1}. The radius of the circular cell is $R = 5$ μm.

the cAMP gradient steepness and where $\bar{S}$ is the average value of S: $\bar{S} = (S_f + S_b)/2$. The steady-state value of the diffusing species B exhibits a mean value proportional to $\bar{S}$ along with a gradient that is proportional to p. An exact steady-state solution of this case is presented in *Supporting Text*, which is published as supporting information on the PNAS web site. It is then possible to derive quadratic equations, depending on the kinetic constants and on p and $\bar{S}$, for A at the front and the back. These equations can easily be solved numerically, and, in Fig. 2A, we have plotted the ratio of A at the front and the back of the cell for the set of parameters of Fig. 1, whereas, in Fig. 2 B and C, we show the value of A at the front and the back, respectively. All quantities are normalized by the activity in the absence of a gradient.

The figure demonstrates that the ratio of A at the front and the back can become quite large, even for rather shallow gradients. This nonlinear behavior can also be understood analytically in the limit of large K, as is worked out in detail in *Supporting Text*. In this limit, we find that at the front of the cell,

$$A_{0,f} \approx \frac{k_a p \bar{S}}{k_{-a}} \left(1 + \frac{k_b L}{2D}\right)^{-1} = \frac{k_{-b}}{k_i} pK \left(1 + \frac{k_b L}{2D}\right)^{-1}. \qquad [4]$$

Thus, ignoring for the moment the last factor, which is typically of order 1, the amplitude at the front has been multiplied by a factor $p\sqrt{K}$. Similarly, for the back, we find

$$A_{0,b} \approx \frac{k_{-b}(1 - p)}{k_i p} \left(1 + \frac{k_b L}{2D}\right), \qquad [5]$$

so that the back has been essentially reduced by the same factor. Note that the level at the back is independent of the mean concentration level $\bar{S}$, meaning that a downstream effector could easily detect which was the back of the cell by a simple thresholding operation. For the ratio of activation between the front and the back, we find

$$\frac{A_{0,f}}{A_{0,b}} \approx \frac{k_a k_i p^2 \bar{S}}{k_{-a}k_{-b}} \left[\frac{1}{(1 + k_b L/(2D))^2(1 - p)}\right]. \qquad [6]$$

Again, the term in the brackets is typically of order 1. The prefactor is just $p^2 K$; so, if K is large, as we assume, the amplification factor is also large, provided that p is not too small.
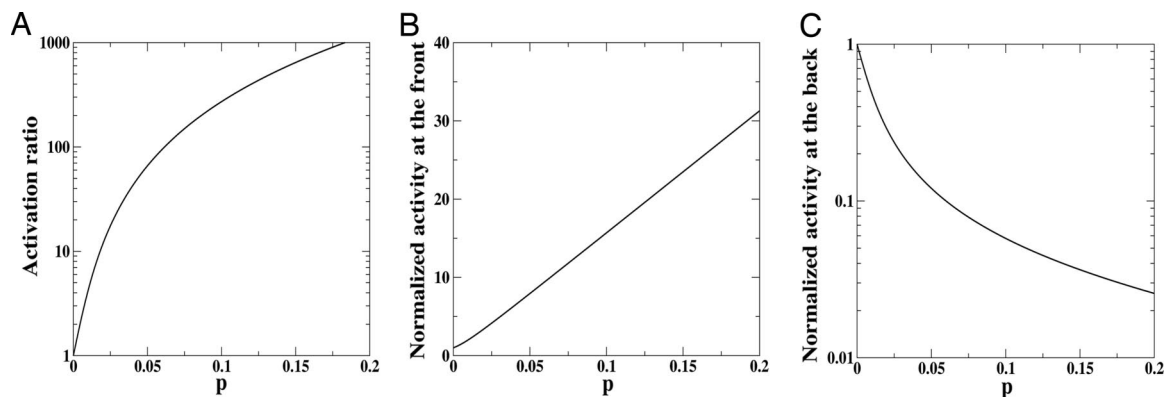
Fig. 2. The ratio of A at the front and the back (*A*), the value of A at the front (*B*), and the value of A at the back (*C*) as a function of the steepness of the gradient parametrized by p. The curves are normalized by the activity of A for a uniform field (i.e., $p = 0$). Parameter values are as in Fig. 1, with $\bar{S} = 1$ molecule per micrometer.

Thus, we find that, to achieve a large ratio between A at the front and back, we need

$$p \gg \frac{1}{\sqrt{K}}. \qquad [7]$$

This analytic result agrees quantitatively with the exact one-dimensional results if K is large enough; (see *Supporting Text*; and see Fig. 5, which is published as supporting information on the PNAS web site). The term in the brackets indicates that insufficient diffusion can kill our effect, because our mechanism relies on diffusion through the cell to communicate between the front and back (see *Supporting Text*; and see Fig. 6, which is published as supporting information on the PNAS web site). However, large diffusion is not sufficient in and of itself, our amplification ratio approaching a finite limit as D gets large.

The above results describe the steady-state response of a one-dimensional version of our model. To fully investigate the dynamics, we simulate the response of our gradient-sensing model, now in two spatial dimensions, to an externally imposed gradient time course. In Fig. 3*A*, we have plotted A as a function of time at the front (black line) and the back (red line) of the circular cell with radius $R = 5$ μm. The initial condition is a uniform concentration of $S = 1$ molecule per μm^2, followed at $t = 0$ s by an instantaneous 10-fold jump in S on one side of our computational box. The value of S on that side is kept constant for the next 50 s while S diffuses through the computational box. The inclusion of a small decay term (0.03 s^{-1}) in the diffusion equation for S leads to an asymmetry between the front and the back of the cell of $\approx$5%. At $t = 50$ s, the gradient is reversed by fixing the value of S at the opposite side of the computational box. The time course of S at the front of the cell and the back of the cell is shown in Fig. 3*B*.

The response of A is initially high all along the perimeter, followed by a rapid decrease at the back of the cell. The final steady state is highly asymmetric and much larger than the external asymmetry: The ratio of A between the back and the front of the cell is >30. The gradient reversal leads rapidly to a reversal of the internal asymmetry. Fig. 3 *C–E* shows A along the cell's perimeter in a grayscale at different times and demonstrates that the shallow gradient in S leads to a large internal asymmetry, further shown in Fig. 3*F*, where we have plotted A and B_m along the perimeter of the cell at $t = 90$ s. Note that the distribution of B_m is opposite from the one of A: B_m displays a maximum at the back of the cell, whereas A exhibits a maximum at the front of the cell. Finally, we plot B at the interior of the cell along the symmetry axis parallel to the gradient for $t = 90$ s. The gradient of B is in the same direction as the external gradient

and is very shallow. As already advertised, these results are exactly as expected from the one-dimensional analysis.

One of the critical experiments that rules out various models of directional sensing relies on stimulating the cell from two different directions. To mimic this condition, we have also considered jumps in the concentration occurring simultaneously on both sides of the computational box. The inclusion of a decay term in the diffusion equation for S leads to two gradients from opposing ends. For the decay constant, we have chosen here (0.1 s^{-1}), which eventually leads to a difference in S of 2% between a membrane point closest to the chemoattractant source (point X in Fig. 4) and a membrane point furthest away from the source (point Y in Fig. 4). Fig. 4*A* shows the response of A to such a gradient stimulus. As is the case for a single gradient stimulus, the response of A shows a large transient, followed by a steady state in which the internal asymmetry is dramatically increased compared with the externally imposed one. This result is further illustrated in Fig. 4*B*, where we have plotted the steady-state response of A along the membrane in a linear grayscale. Finally, we have verified that the same final state can be reached even if the two jumps do not occur simultaneously or if the jumps have unequal magnitudes (data not shown).

Discussion

Comparison to Experimental Data. The model we have presented here describes the initial internal response to externally imposed signals. All subsequent responses are downstream from our model, including the experimentally determined localization of PH-domain proteins and the localized activation of Ras. Thus, our model serves as input to downstream modules and can be compared, with suitable assumptions, with experiments. For example, in the uniform-stimulus case, a sudden increase in the external chemoattractant concentration leads to a rapid uniform response (see Fig. 1), as indeed observed in the experiments (12, 13, 15). This response is followed by a gradual drop to low levels that can be assumed to be translated into a loss of response (i.e., membrane localization) in the downstream modules. The time scale of the response depends on the model parameters and the downstream modules and can readily be made consistent with experimental findings (Fig. 1). We note, in passing, that this approach could also account for the generation of spontaneously appearing patches along the cell's membrane if the steady-state output of our model drives a Turing-pattern mechanism in the downstream modules (28, 29); here, we do not pursue this added complication any further.

When exposed to a shallow gradient, our model is able to create a large internal asymmetry that can be rapidly reversed (see Fig. 3). Furthermore, upon introduction of the gradient,
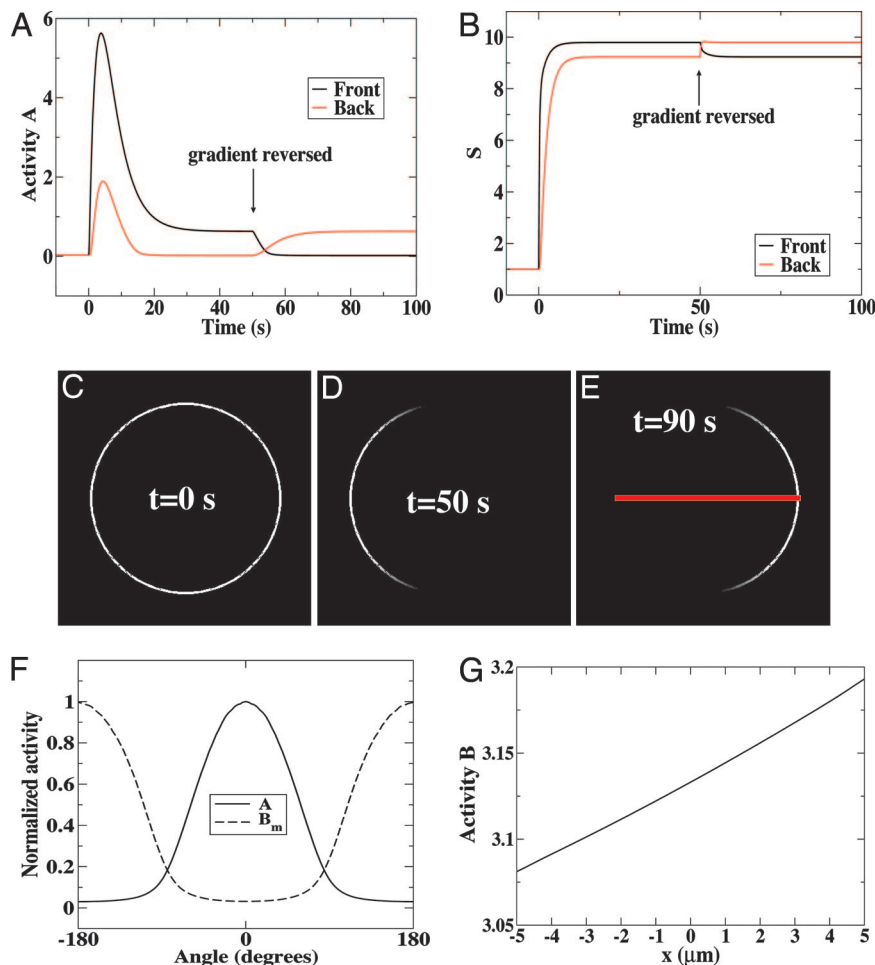
Fig. 3. The response of the model to a gradient stimulus. (*A*) The value of *A* as a function of time at the front of the cell (black line) and the back of the cell (red line) as a response to a gradient reversal experiment. (*B*) The external concentration (*S*) before and after gradient reversal at *t* = 50 s. (*C–E*) Value of *A* along the perimeter of the cell in a linear grayscale at different times. (*F*) Values of *A* and B_m, normalized by their maximum value, along the perimeter at *t* = 90 s. (*G*) Value of *B* as a function of space measured along the symmetry axis of the cell, parallel to the gradient (drawn as a red line in *E*). Parameter values are as in Fig. 1, with the decay constant of *S* chosen to be 0.03 s^{-1} and a diffusion constant equal to 100 μm$^2 \cdot$s^{-1}.

both the back and the front of the cell respond, followed by a loss of response at the back, as seen in the experiments (12, 14). The time scale of the response of *A* at the back of the cell, as well as its dynamics upon a gradient reversal, is determined in large part

Fig. 4. The response of the model to multiple sources. (*A*) The dynamics of the response of our model to two opposing gradient sources. The value of *S* at two opposing sides of the computational box is changed from 1 to 10 molecules per micrometer at *t* = 0 s and kept constant. The inclusion of a decay constant (0.1 s^{-1}) results in steady state in a difference in *S* of 2% along the membrane. (*B*) The steady-state response of *A* shown in a linear grayscale.

by the value of the diffusion constant of *B*. A small value of the diffusion constant will lead to slow dynamics, whereas a large value leads to fast loss of activation at the back and a fast reversal. Fig. 3 shows that the time scales in our model can be consistent with experimental findings (14). Of course, the dynamics of the read-out signal depend also on the details of the specific read-out module, and an exact comparison with kinetic experiments requires additional knowledge of the pathways involved.

Contrary to previous theoretical efforts (20, 23, 24, 30), the response of the model, measured in terms of the variable *A*, is not a simple amplification of the external gradient. Instead, the response should be compared with a switch: The front, i.e., the side of the membrane closest to the chemoattractant source, has a high level of *A*, whereas the back has a very low level. For a wide range of parameters, this gradient leads to an internal asymmetry that is much larger than the external one (Fig. 2), as reported in the literature (14). Moreover, the level at the back is independent of the external signal (see Eq. **5**), leading to the complete suppression of the signal at the back of the cell for a large range of gradients.

Our model is also able to replicate experiments in which cells are exposed to multiple simultaneous sources (14). As can be seen in Fig. 4, two gradients imposed from opposite sides of the
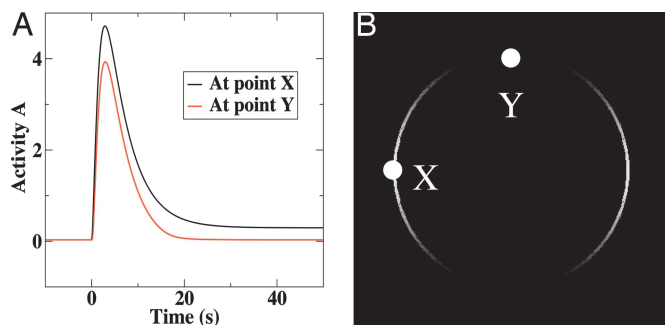
cell lead to a response that shows a maximum at both of the two locations closest to the source. Because our mechanism does not rely on an instability, it can lead to two spatially separate maxima, even if the sources have unequal strength or are applied at different times (data not shown).

Mechanism Underlying the Model. How is this large, switch-like and rapidly reversible asymmetry achieved? The key elements in our model are the equal production of A and B, together with a sufficiently large diffusion constant of the cytosolic component and sufficiently slow decays. Without cytosolic diffusion, the equal production of A and B would result in values of A and B that are proportional to the external gradient. The inclusion of cytosolic diffusion for B, however, leads to an almost constant concentration of B throughout the cell. Thus, the initial value of A will be higher than B at the front but lower at the back. The third component in our model, the membrane-bound B_m, inactivates A and is proportional to B. The final result is a nearly complete inactivation at the back but not at the front. In other words, this "balanced inactivation" is able to translate a shallow external gradient into a state in which the front and the back are completely different. The internal asymmetry can be reversed rapidly, provided the diffusion coefficient of the cytosolic component (B) is large enough. In *Supporting Text*, we present results that show the dependence of our mechanism on this diffusion constant. There, we also show that our mechanism is robust against model variations, including the incorporation of membrane diffusion for A and B_m (Fig. 7, which is published as supporting information on the PNAS web site) and the inclusion of membrane desorption of B_m (Fig. 8, which is published as supporting information on the PNAS web site).

Possible Biochemical Components. The biochemical steps in the pathway between receptor binding and the experimental read-out variables are not completely known, and, hence, it is difficult to identify our model components in a definitive way. However, our main assumption, equal production of A and B, suggests a heterotrimeric G protein as a possible candidate. G proteins are complexes of three proteins, G_α, G_β, and G_γ, and are involved in numerous second-messenger cascades (31). In *Dictyostelium*, at least 11 α-subunits have been identified along with one β- and one γ-subunit that are tightly bound (32). Upon cAMP binding to the CAR1 receptor, GTP can be exchanged for GDP on the G_α subunits, leading to the dissociation of the G protein complex into G_α and $G_{\beta\gamma}$. Both of these subunits are involved in downstream signaling (33), and genetic studies have demonstrated that the $G_{\beta\gamma}$ complex is essential for chemotaxis (34, 35). Recent research has demonstrated that this complex is found both at the membrane and in the cytosol (36, 37). Its cytosolic diffusion constant was found to be $D \approx 10 \ \mu m^2/s$ (37), large enough to ensure a fast reversal of the internal asymmetry in our model. Furthermore, its subcellular organization does not show a significant amplification of the external gradient, indicating that the directional sensing step is downstream from the G protein disassociation (36). The signaling cycle is completed through the activity of GTPases that hydrolyze the bound GTP on the G_α, facilitating the recombination of G_α and $G_{\beta\gamma}$. Taken together, these data suggest that we might be able to identify the model component A with G_α and the model component B with $G_{\beta\gamma}$. $G_{\beta\gamma}$ would then be the inhibitor, and G_α, in both its GTP-bound and GDP-bound form, would play the role of activator and would be coupled to the downstream modules responsible for Ras and PH-domain protein localization. Unfortunately, current experimental findings are unable to provide enough details of these pathways to definitively evaluate this scenario. In neutrophils, experiments have demonstrated that $G_{\beta\gamma}$ mediates the activation of one PI3K (class I_B PI3Kγ) (38), whereas, in *Dictyostelium*, $G_{\beta\gamma}$ is responsible for adenylyl cyclase activation and actin polymer-

ization (34, 39). However, it is currently not known how other PI3Ks or Ras are activated. We should point out that our mechanism affords a natural role of $G_{\beta\gamma}$ in the activation of certain pathways. After all, $G_{\beta\gamma}$ has an opposite localization pattern from G_α (Fig. 3F), suggesting that $G_{\beta\gamma}$ might be involved in the pathways of proteins that localize in the back, including ACA, PTEN, PAKa, and Myosin II (9). This specific realization of our model naturally solves the problem of how to ensure the proper balance between activation and inhibition in the system. Balance occurs naturally because activation and inhibition are both created by G protein disassociation. We should point out the alternate possibility of an additional feedback mechanism that ensures balanced inactivation without equal A and B production rates; it is, indeed, possible to construct such a model (data not shown).

As with all other theoretical models, our mechanism depends on the activity of an inhibitor. Without this inhibitor, it is difficult to imagine terminating and adapting the signal response. The biochemical identification of these inhibitors has proven to be difficult despite intensive experimental work. Of course, it is always possible that there exists a hitherto undiscovered molecule that plays the role of inhibitor in the directional sensing mechanism. But, at least at present, an additional appeal of our tentative identification of a G protein as supplying both the inhibitor and the activator is that this model eliminates the need for such an unknown component.

Predictions of the Model. The predictions offered by our mechanisms can be separated into two types. The first type is independent of the exact biochemical details and is based on the phenomenological aspects of the model. In particular, our model predicts that the response of cells to shallow gradients is switch-like for a large range of gradients and average background levels of chemoattractant. A switch-like response was recently observed in experiments for one particular gradient strength (14). Unfortunately, it is currently difficult to control quantitatively the steepness and the background level of the external gradient. However, the experimental techniques made possible by microfluidic designs (5, 40) offer hope that a systematic study of the response of cells in well controlled gradient environments will soon become possible. Clearly, it would be very interesting to measure quantitatively the membrane distribution of PH-domain proteins and Ras in cells after sudden exposure to well characterized gradients. Because our directional sensing model is upstream from the pathways responsible for polarization, the switch-like behavior should be observable in latrunculin-treated cells in which F-actin polymerization is abolished.

The second type of prediction depends on our tentative identification of a heterotrimeric G protein as the key component in the model. In fact, if this G protein generates both the activator and inhibitor, our model predicts that G_β null mutants would not exhibit the switch-like behavior of Fig. 2. Because signaling through this protein is upstream from the usual readout components, a drastically altered localization pattern of PH-domain proteins and Ras would follow. Perhaps the strongest prediction is that it would have to be the α-subunit that directs the "frontness" pathway and the $\beta\gamma$-subunit that controls the back. Furthermore, the α-subunit would have to remain active, even in its GDP-bound form, as long as it has not reassociated with the $\beta\gamma$-subunit.

Methods

The Model. For simplicity, we will ignore the details of the binding process of the chemoattractant to the receptors and will assume that the concentration of activated receptors, S, is directly related to the chemoattractant concentration. These activated receptors produce a membrane-bound species A and a cytosolic

PHYSICS

species B at equal rates k_a. The cytosolic species diffuses inside the cell and can attach itself to the membrane at a rate k_b, where we will label it B_m. There, it can inactivate A with rate k_i, a process that will be assumed to be irreversible. Thus, A plays the role of activator, and B plays the role of inhibitor in our model. Finally, we will allow for the spontaneous degradation of A and B_m at rates k_{-a} and k_{-b}, respectively. These rates will be taken to be small compared with both the activation and the recombination. In mathematical terms, these reactions are written as

$$\frac{\partial A}{\partial t} = k_a S - k_{-a} A - k_i A B_m \text{ at the membrane,}$$

$$\frac{\partial B_m}{\partial t} = k_b B - k_{-b} B_m - k_i A B_m \text{ at the membrane, and} \quad \textbf{[8]}$$

$$\frac{\partial B}{\partial t} = D \nabla^2 B \text{ in the cytosol,}$$

with a boundary condition for the outward pointing normal derivative of the cytosolic component

$$D \frac{\partial B}{\partial n} = k_a S - k_b B. \quad \textbf{[9]}$$

Numerical Method. The above equations are solved on a two-dimensional circular geometry by using the phase-field method. The phase-field is an auxiliary construct that allows for a smooth interpolation between the interior and exterior of the cell. This approach enables the accurate simulation of intra- and extracellular dynamics in complex geometries, by using simple Cartesian grids (41, 42). The cell is placed in a computational box measuring 40×40 grid points and a grid spacing of $0.25\ \mu$m. The cell's diameter was chosen to be $5\ \mu$m. We have verified that smaller grid spacings do not lead to qualitatively different results (data not shown). Differences in S along the cell wall are produced by introducing a diffusing field C, (proportional to the cAMP concentration), fixing its value on one of the boundaries of the computational box and by solving the diffusion equation (D_c is taken to equal $100\ \mu$m^2/sec), with a degradation term for C in the space outside the cell. The value of S is taken to be the value of C in the cell wall.

1. Clark, R. (1996) *The Molecular and Cellular Biology of Wound Repair* (Plenum, New York).
2. Dormann, D. & Weijer, C. J. (2003) *Curr. Opin. Genet. Dev.* **13**, 358–364.
3. Condeelis, J., Singer, R. H. & Segall, J. E. (2005) *Annu. Rev. Cell Dev. Biol.* **21**, 695–718.
4. Zigmond, S. H. (1977) *J. Cell. Biol.* **75**, 606–616.
5. Song, L., Nadkarni, S. M., Bödeker, H. U., Beta, C., Bae, A., Franck, C., Rappel, W.-J., Loomis, W. F. & Bodenschatz, E. (2006) *Eur. J. Cell Biol.*, in press.
6. Rosoff, W. J., Urbach, J. S., Esrick, M. A., McAllister, R. G., Richards, L. J. & Goodhill, G. J. (2004) *Nat. Neurosci.* **7**, 678–682.
7. Bourne, H. R. & Weiner, O. (2002) *Nature* **419**, 21.
8. Chung, C. Y. & Firtel, R. A. (2002) *J. Muscle Res. Cell Motil.* **23**, 773–779.
9. Manahan, C. L., Iglesias, P. A., Long, Y. & Devreotes, P. N. (2004) *Annu. Rev. Cell Dev. Biol.* **20**, 223–253.
10. Postma, M., Bosgraaf, L., Loovers, H. M. & Haastert, P. J. V. (2004) *EMBO Rep.* **5**, 35–40.
11. Devreotes, P. & Janetopoulos, C. (2003) *J. Biol. Chem.* **278**, 20445–20448.
12. Parent, C. A., Blacklock, B. J., Foehlich, W. M., Murphy, D. B. & Devreotes, P. N. (1998) *Cell* **95**, 81–91.
13. Meili, R., Ellsworth, C., Lee, S., Reddy, T. B., Ma, H. & Firtel, R. A. (1999) *EMBO J.* **18**, 2092–2105.
14. Janetopoulos, C., Ma, L., Devreotes, P. N. & Iglesias, P. A. (2004) *Proc. Natl. Acad. Sci. USA* **101**, 8951–8956.
15. Sasaki, A. T., Chun, C., Takeda, K. & Firtel, R. A. (2004) *J. Cell Biol.* **167**, 505–518.
16. Funamoto, S., Meili, R., Lee, S., Parry, L. & Firtel, R. A. (2002) *Cell* **109**, 611–623.
17. Huang, Y. E., Iijima, M., Parent, C. A., Funamoto, S., Firtel, R. A. & Devreotes, P. (2003) *Mol. Biol. Cell* **14**, 1913–1922.
18. Iijima, M. & Devreotes, P. (2002) *Cell* **109**, 599–610.
19. Meili, R., Sasaki, A. T. & Firtel, R. A. (2005) *Nat. Cell Biol.* **7**, 334–335.
20. Meinhardt, H. (1999) *J. Cell Sci.* **112**, 2867–2874.
21. Narang, A., Subramanian, K. K. & Lauffenburger, D. A. (2001) *Ann. Biomed. Eng.* **29**, 677–691.
22. Postma, M. & van Haastert, P. J. M. (2001) *Biophys. J.* **81**, 1314–1323.
23. Levchenko, A. & Iglesias, P. A. (2002) *Biophys. J.* **82**, 50–63.
24. Rappel, W. J., Thomas, P. J., Levine, H. & Loomis, W. F. (2002) *Biophys. J.* **83**, 1361–1367.
25. Parent, C. A. & Devreotes, P. N. (1999) *Science* **284**, 765–770.
26. Turing, A. (1952) *Phil. Trans. R. Soc. London B* **237**, 37–72.
27. Subramanian, K. K. & Narang, A. (2004) *J. Theor. Biol.* **231**, 49–67.
28. Postma, M., Roelofs, J., Goedhart, J., Gadella, T. W., Visser, A. J. & Haastert, P. J. V. (2003) *Mol. Biol. Cell* **14**, 5019–5027.
29. Postma, M., Roelofs, J., Goedhart, J., Loovers, H. M., Visser, A. J. & Haastert, P. J. V. (2004) *J. Cell Sci.* **117**, 2925–2935.
30. Ma, L., Janetopoulos, C., Yang, L., Devreotes, P. N. & Iglesias, P. A. (2004) *Biophys. J.* **87**, 3764–3774.
31. Gilman, A. G. (1987) *Annu. Rev. Biochem.* **56**, 615–649.
32. Brzostowski, J. A., Johnson, C. & Kimmel, A. R. (2002) *Curr. Biol.* **12**, 1199–1208.
33. Janetopoulos, C., Jin, T. & Devreotes, P. (2001) *Science* **291**, 2408–2411.
34. Jin, T., Amzel, M., Devreotes, P. N. & Wu, L. (1998) *Mol. Biol. Cell* **9**, 2949–2961.
35. Zhang, N., Long, Y. & Devreotes, P. N. (2001) *Mol. Biol. Cell* **12**, 3204–3213.
36. Jin, T., Zhang, N., Long, Y., Parent, C. A. & Devreotes, P. N. (2000) *Science* **287**, 1034–1036.
37. Ruchira (2005) Ph.D. thesis (Wageningen Universiteit, Wageningen, The Netherlands).
38. Brock, C., Schaefer, M., Reusch, H. P., Czupalla, C., Michalke, M., Spicher, K., Schultz, G. & Nurnberg, B. (2003) *J. Cell Biol.* **160**, 89–99.
39. Wu, L., Valkema, R., Haastert, P. J. V. & Devreotes, P. N. (1995) *J. Cell Biol.* **129**, 1667–1675.
40. Jeon, N. L., Baskaran, H., Dertinger, S. K., Whitesides, G. M., de Water, L. V. & Toner, M. (2002) *Nat. Biotechnol.* **20**, 826–830.
41. Kockelkoren, J., Levine, H. & Rappel, W. J. (2003) *Phys. Rev. E* **68**, 037702.
42. Levine, H. & Rappel, W. J. (2005) *Phys. Rev. E* **72**, 061912.